Electronic Supplementary Material (ESI) for Nanoscale Horizons.

Efficient photogeneration of nonacene on nanostructured graphene

Cosme G. Ayani, Michele Pisarra, José I. Urgel, Juan Jesús Navarro, Cristina Díaz, Hironobu Hayashi, Hiroko Yamada, Fabian Calleja, Rodolfo Miranda, Roman Fasel, Fernando Martín, Amadeo L. Vázquez de Parga

I. Gas phase molecular orbitals of nonacene.

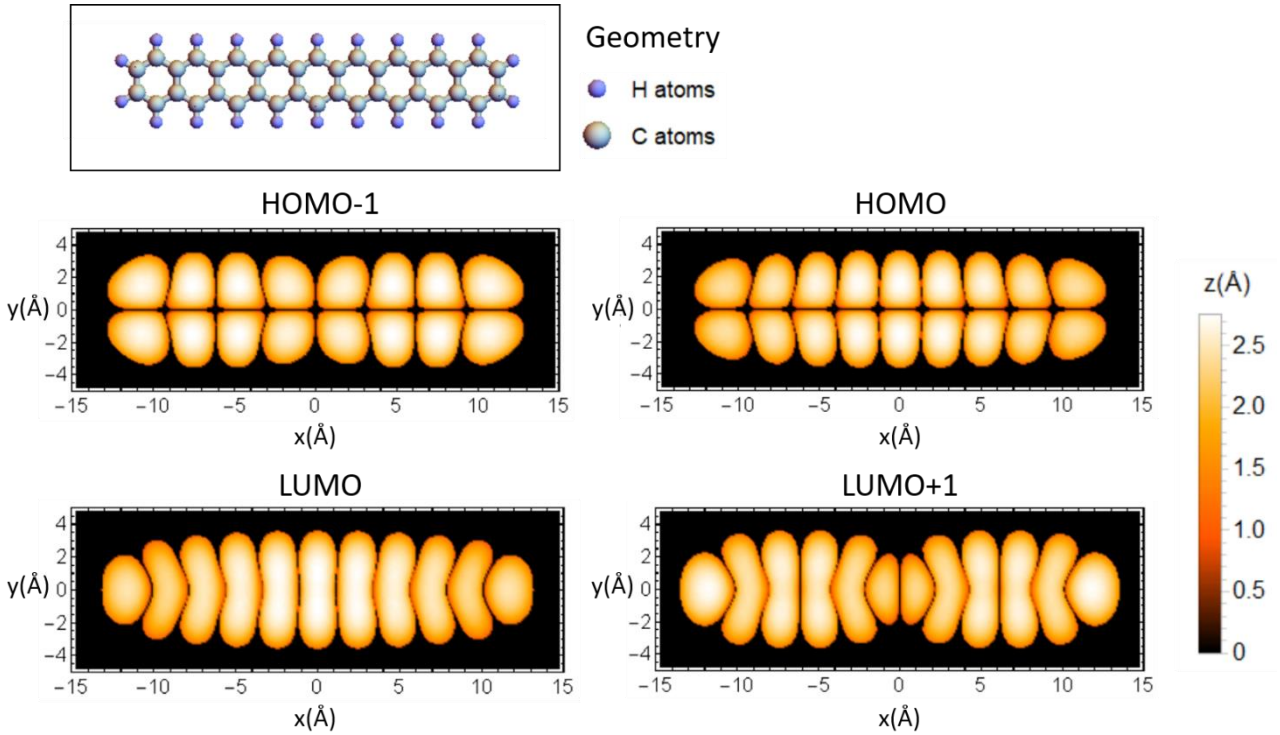

Figure S1: Gas phase molecular orbitals of nonacene. The plots represent simulated STM images to ease comparison with Fig. 2 of the main text. The isosurface $\rho = 6.3 \times 10^{-5}\text{Å}^{-3}$ has been chosen, which corresponds to a tunneling current of $I_t = 0.1$nA when a single Molecular Orbital is included in the integration window. The origin of the z scale is set on the molecular plane. The box-size is the same for all the figures.

II. Large scale images after the light exposure

In order to get an estimation of the conversion yield of the precursor molecules after light irradiation we have investigated different locations of the sample. We took large-scale images with enough resolution to be able to distinguish between the nonacenes and the α-bisdiketone nonacene precursor. Figure S2 shows two representative large-scale images used to obtain the statistics for the conversion yield. In these images, we only observe nonacene molecules in the defect-free areas of gr/Ru. We have discarded from the statistical analysis the molecules appearing near surface defects, since, in most of the cases, the observed molecular species could not be attributed to either nonacene or the precursor. Most likely, these unusual molecular species are not produced by light but by the strong interaction of nonacenes (or the precursors) with the very reactive defect areas. Therefore, they must be excluded from the evaluation of the light-conversion yield, which according to these images is 100%. It is also worth mentioning that the deposition of the precursor molecules and light conversion experiments were carried out four times with reproducible results.

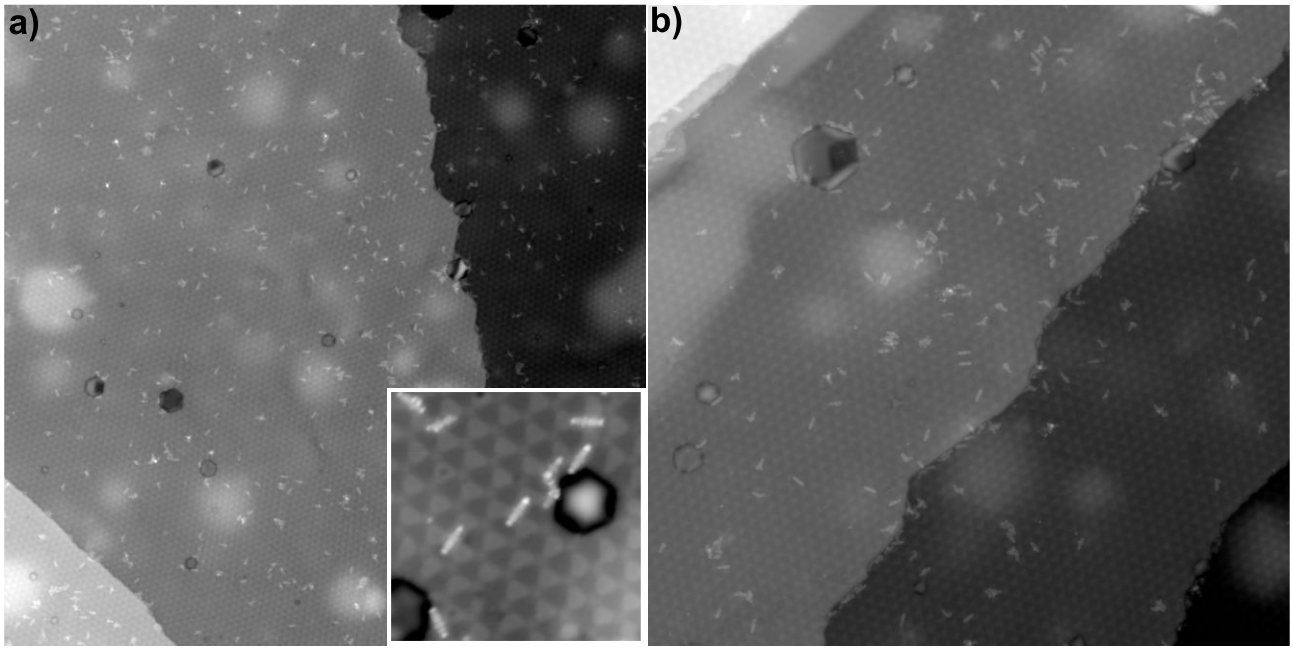

Figure S2: (a) Large scale STM image 300 nm x300 nm (1.7V, 100pA). The inset shows a high-resolution image (25 nm x 25 nm, 1.7V, 100pA) where some nonacene molecules without α-bisdiketone functional groups attached can be resolved. (b) Another large scale STM image 150 nm x 150 nm (1.7V, 100pA) measured on a different location on the sample.

III. Optical properties of Au(111), Ru(0001) and graphene

To understand the main differences in the optical properties of the Ru(0001) and Au(111) surfaces, it is useful to first look at their electronic properties. Such a comparison is carried out in Fig. S3 in which we report the band structure, as obtained in a DFT calculation, of model surfaces for gold and for ruthenium. The surfaces are modeled by 15 layer thick slabs oriented in the (111) direction for gold and in the (0001) direction for ruthenium. For comparison, we also report the bulk band structure for both materials along the same path in the irreducible Brillouin zone. From a comparison between the bulk band structure and that of the slab, one can see that the 15-layer model surface reproduces the gold surface state located at ~ -0.4 eV, at the Γ point.

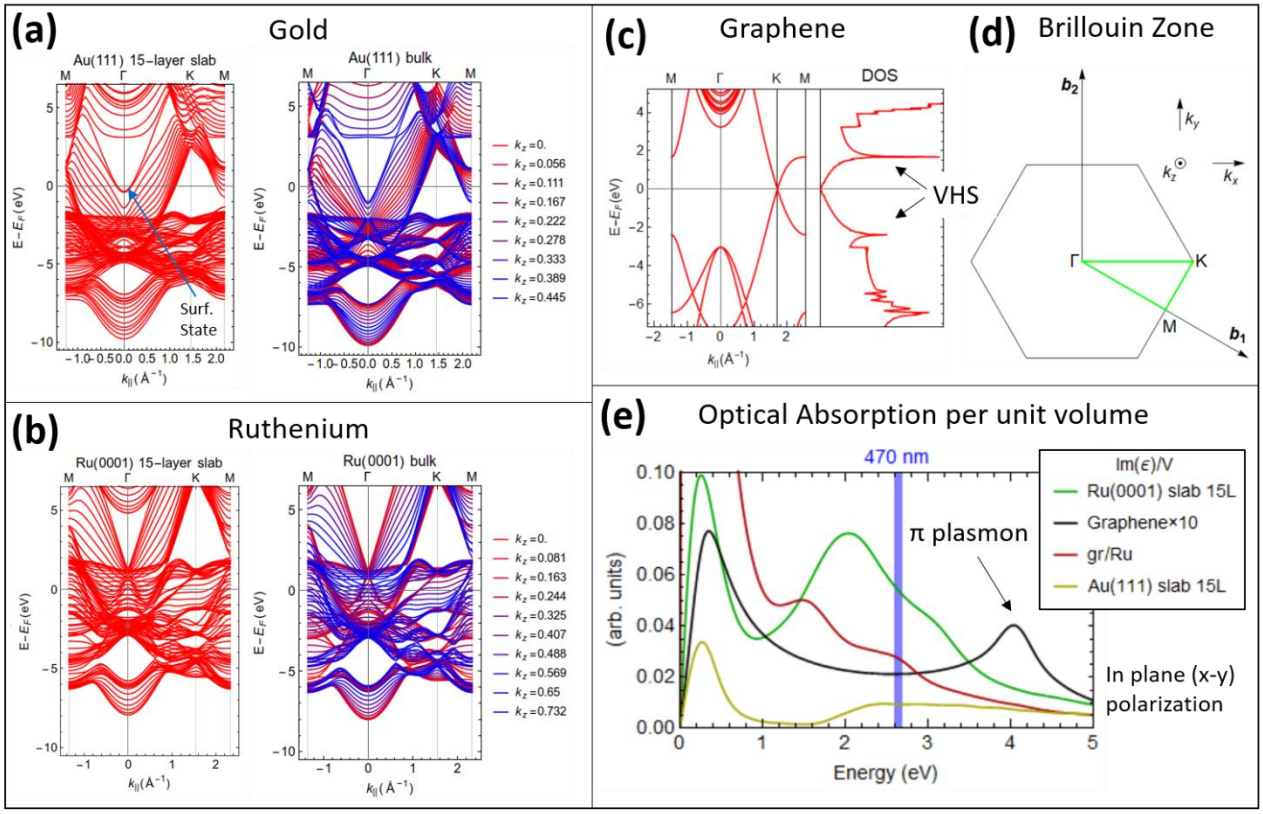

Figure S3: Band structure of (a) Au(111) and (b) Ru(0001) obtained for a model surface (15 layer thick slab) and the bulk material, along a high symmetry Brillouin zone path. In panel a, the gold surface state at -0.4 eV at the Γ point is highlighted. (c) Band structure and density of states of monolayer graphene; the two Van Howe singularities (VHS), generated by the flat dispersion of the π and π^* bands at the M point, are highlighted in the DOS plot. (d) 2D Brillouin Zone, with the high symmetry path employed in the band plot (highlighted in green). (e) Imaginary part of the dielectric function, $Im[\epsilon(\omega)]$, per unit volume, representing the optical properties of the analyzed materials, as obtained in a Linear Response TD-DFT calculation; we multiplied the graphene results by 10 to visualize them on the same scale as Au and Ru; the vertical blue gridline marks the energy position of the light used in the experiment.

The main difference between Au(111) and Ru(0001) band structures is represented by the *d* bands. In the Au(111) case, the *d* manifold is completely filled and extends in the energy range $[-7, -2]$ eV, whereas *sp* bands cross the Fermi level. On the other hand, in Ru(0001), the *d* bands are only partially filled, and extend over the energy range $[-6,2]$ eV, thus crossing the Fermi level. Such differences are directly reflected in the optical properties of

the two surfaces, which are compared in Fig. S3e. In the same panel we also include the graphene optical properties. At the low energy end the spectra are dominated by the so-called Drude peak, which is present due to the conducting nature of the analyzed materials. The graphene spectrum is then characterized by an adsorption peak at ~ 4 eV, which corresponds to a strong transition between the two Van Howe singularities at ~ -2 eV and ~ 2 eV, generated by the flat dispersion of the π and π* bands at the M point (see Fig. S3c). This peak is the ($\boldsymbol{q} \to 0$) one-body counterpart of the so-called π-plasmon, which is typical of graphene and graphitic materials. This last observation demonstrates that the TD-DFT approach adopted here reproduces qualitatively well the features of the light adsorption spectrum. Now we turn our attention to the Au spectrum, for which we can identify a plateau in the light adsorption starting at ~ 2 eV, which corresponds to the onset of interband transition from the *d* bands. Finally we observe that the Ru(0001) spectrum presents additional peaks not appearing in Au and an overall higher intensity. These features are due to the empty *d* bands, which increase the density of final states for low excitation energies, thus causing a higher light adsorption as compared to gold. We finally observe that, once the gr/Ru interface is formed, the optical properties of the two materials are combined. It is important to note that, due to the very large in-plane unit cell needed to describe the gr/Ru moiré, this TD-DFT calculation has been carried out by only using three Ru layers, so that the results can only be used for a qualitative analysis. These results show that the gr/Ru spectrum exhibits a double peak structure reminiscent of the Ru(0001) spectrum, whereas the feature of the graphene spectrum, which as observed is at least one order of magnitude less intense than the Ru(0001) one, are not easily identified in the gr/Ru spectrum, as expected.

We conclude our analysis on the optical properties of gr/Ru by comparing the optical absorption calculated for the gr/Ru system with and without the precursor molecule. Such a comparison is carried out in Fig.S4a. As expected, the two spectra are almost perfectly identical, meaning that the precursor molecule absorption is negligible as compared with the gr/Ru one. Finally, we report in Fig.S4b the optical absorption of the precursor molecule in gas phase. We analyzed two different geometries (see Fig.S4c). The “optimized” geometry is obtained after a full relaxation of the coordinates of all the atoms for the precursor molecule in gas phase. Due to the presence of the diketone groups the precursor molecule presents a heavily bent geometry. On the other hand, the “distorted” geometry is the one that the precursor molecule adopts when adsorbed on gr/Ru. We notice that in the latter case, the backbone of the precursor molecule is almost flat. Interestingly, we observe that the spectrum of the optimized geometry exhibits a prominent adsorption peak at the photon energy used in the experiment, but its intensity is reduced by approximately a factor of two in the spectrum of the distorted molecule.

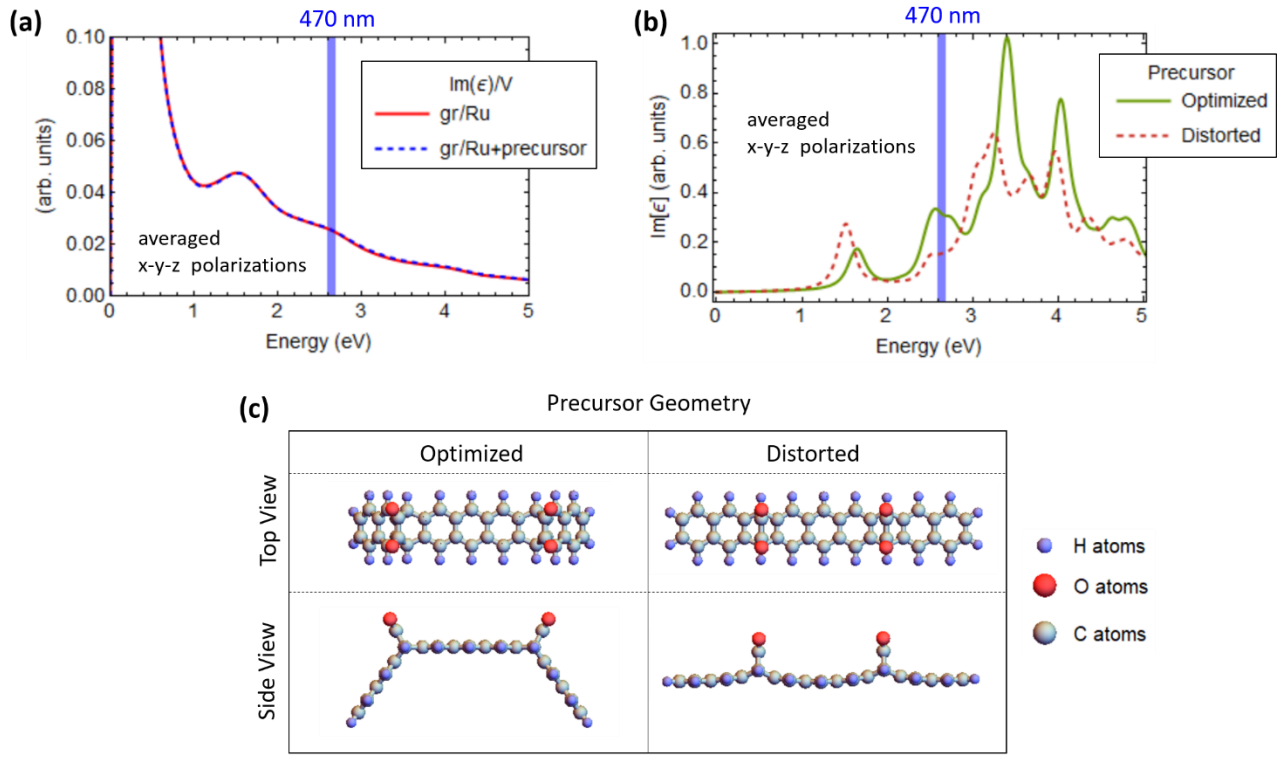

Figure S4: (a) Imaginary part of the dielectric function, $Im[\epsilon(\omega)]$, per unit volume, averaged over all the polarization directions, for gr/Ru and the gr/Ru+precursor systems; the same vertical scale as in Fig. S3e is used. (b) Imaginary part of the dielectric function averaged over the three polarization directions, for the two different geometries given in (c) of the precursor molecule in gas phase; notice that the same normalization convention for the two spectra are used but they are not to scale with the spectra given in panel a. (c) Top view and side view of the geometries of the precursor molecule used in the calculation of panel b.